Geoneutrino Detection
KamLAND
Borexino
SNO+
Upcoming
JUNO
JNE
OBD
$\bar{\nu}$ Directionality
Towards ^{40}K
e^- elastic
Gas TPC
ν-nuclei capture
Low-threshold IBD
Summary

Geoneutrino Experiments and Prospects

Benda Xu
thanks to Wentai Luo and Xuewei Liu

University of Chinese Academy of Sciences

2026-11-13 School of Neutrino Geoscience at Zhuhai China

Geoneutrino Detection
KamLAND
Borexino
SNO+
Upcoming
JUNO
JNE
OBD
$\bar{\nu}$ Directionality
Towards ^{40}K
e^- elastic
Gas TPC
ν-nuclei capture
Low-threshold IBD
Summary

Outline

1. Geoneutrino Detection
2. KamLAND
3. Borexino
4. SNO+
5. Upcoming
   - JUNO
   - JNE
   - OBD
6. $\bar{\nu}$ Directionality
7. Towards ^{40}K
   - e^- elastic
   - Gas TPC
   - ν-nuclei capture
   - Low-threshold IBD
8. Summary

Geoneutrino Experiments and Prospects
Benda Xu
Geoneutrino Detection
KamLAND
Borexino
SNO+
Upcoming
JUNO
JNE
OBD
$\bar{\nu}$ Directionality
Towards ^{40}K
e^- elastic
Gas TPC
ν-nuclei capture
Low-threshold IBD
Summary

Geoneutrino Detection

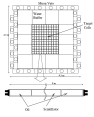
Motivation

Extract more insights on geological models from geoneutrinos

- Cosmogenic background;
- Radiactive background and Fiducial volume;
- Suppressing Reactor neutrino (better constrain, move a away, shutdown, etc.)
- Get bigger.

Liquid detector media

Medium	Advantages	Limitations
Liquid scintillator	Well tested. Good energy resolution with fewer light sensors.	Combustible. Must be shipped or produced on site.
Water with gadolinium (Gd)	Water is nontoxic and widely available. Its clarity allows large detectors.	More light sensors. Poorer energy resolution and background rejection.
Water-based liquid scintillator with Gd	Uses less organic liquid. Tuning the mixture can improve background rejection over water.	Less experience at large scale.



Palo Verde
Gd-loaded scintillator, 180 t



KamLAND
Liquid scintillator, 1 kt



Super-Kamiokande
Gd-loaded water, about 50 kt

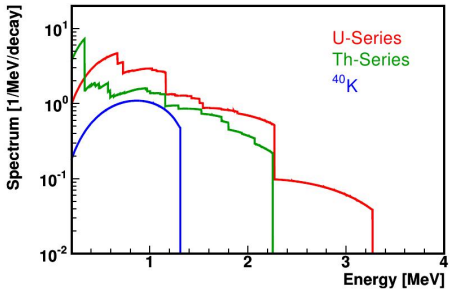
U/Th as weak interaction probe into the Earth

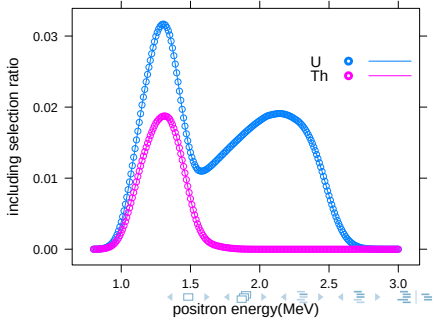
$$^{238}\mathrm{U} \longrightarrow {}^{206}\mathrm{Pb} + 8\,\alpha + 6\,\mathrm{e}^- + 6\,\bar{\nu}_e \qquad + 51.698\,\mathrm{MeV}$$

$$^{232}\mathrm{Th} \longrightarrow {}^{208}\mathrm{Pb} + 6\,\alpha + 4\,\mathrm{e}^- + 4\,\bar{\nu}_e \qquad + 42.652\,\mathrm{MeV}$$

$$^{40}\mathrm{K} \xrightarrow{89.3\,\%} {}^{40}\mathrm{Ca} + \mathrm{e}^- + \bar{\nu}_e \qquad + 1.311\,\mathrm{MeV}$$

$$^{40}\mathrm{K} + \mathrm{e}^- \xrightarrow{10.7\,\%} {}^{40}\mathrm{Ar} + \nu_e \qquad + 1.505\,\mathrm{MeV}$$

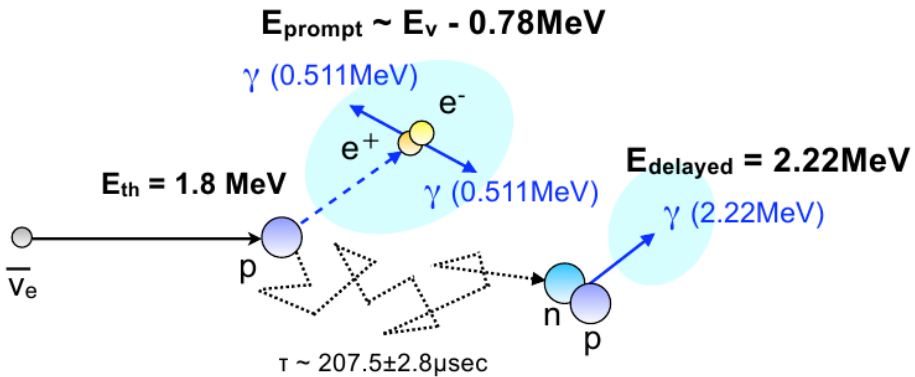




Antineutrino Detection: Inverse Beta Decay

$$\bar{\nu}_e + \mathrm{p} \longrightarrow \mathrm{e}^+ + \mathrm{n}$$

- Kinetic energy mostly to e^+, E^+ in good correlation with E_ν.
- Energy threshold 1.8MeV, cannot detect $\bar{\nu}_e$ from ^{40}K, U/Th only.
- Delayed coincidence



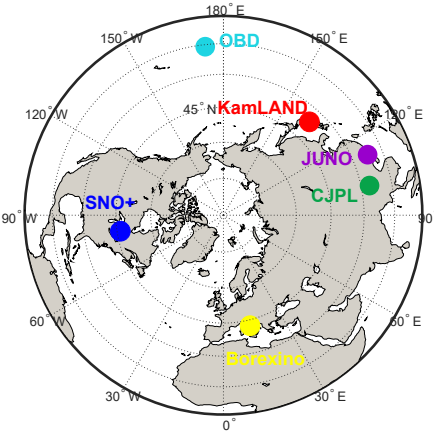
Heat from uranium and thorium

Each site measures a different mix of crust and mantle. A model of U and Th in the Earth relates the local rate to global heat production.

Experiment	First result	Heat (TW)
KamLAND (Japan)	2005	$15.4^{+8.9}_{-7.9}$
Borexino (Italy)	2010	$31.3^{+13.6}_{-12.7}$
SNO+ (Canada)	2025	47^{+47}_{-43}

Years mark the first geoneutrino result. Heat estimates are from August 2025, with SNO+ using its first data set.

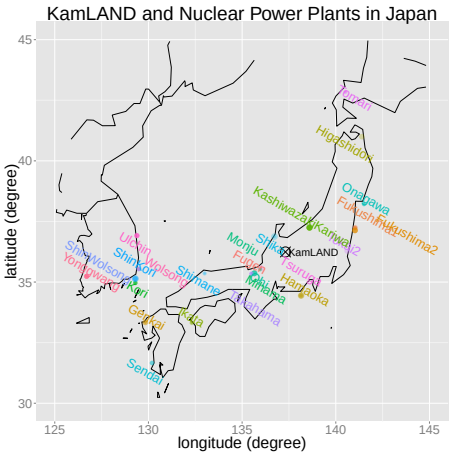
McDonough (TAUP 2025), slide 8.

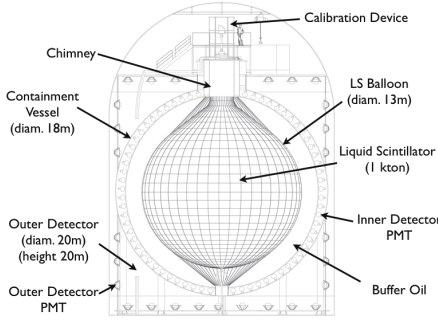


KamLAND

Facts

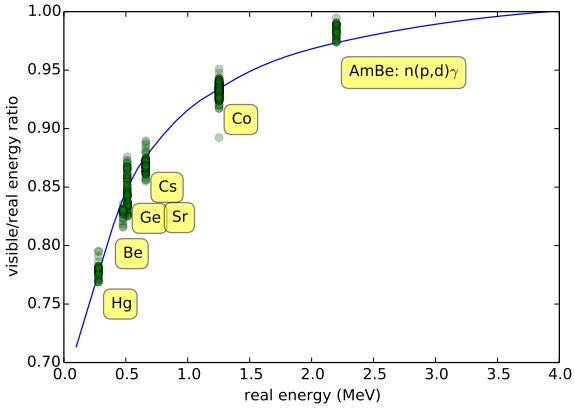
- 1 kton of liquid scitillator, $34\,\%$ PMT coverage





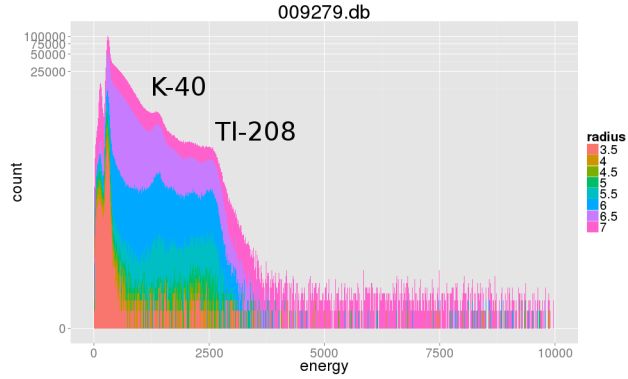
Calibrations

- PMT by laser: time delay and 1 photo-election
- light yield, energy scale, energy-vertex dependency and vertex bias ^{203}Hg, ^{7}Be, ^{85}Sr, ^{137}Cs, ^{65}Zn, ^{68}Ge, ^{60}Co
- delayed coincidence ^{241}Am^{9}Be, ^{210}Po^{13}C



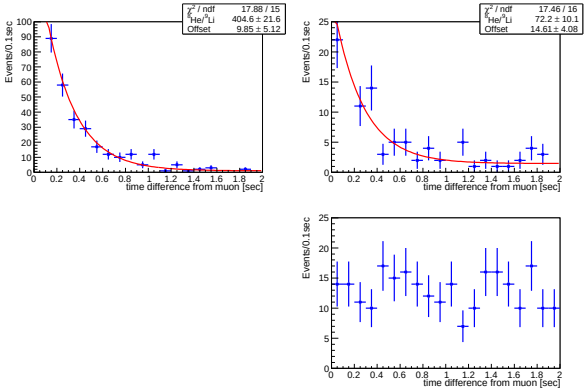
Flasher, Noise and Fiducial Volume

- Flasher: discharge of PMT
- Noise: PMT hit timing does not cluster
- radius R<6m to reject accidental and (α, n) sources



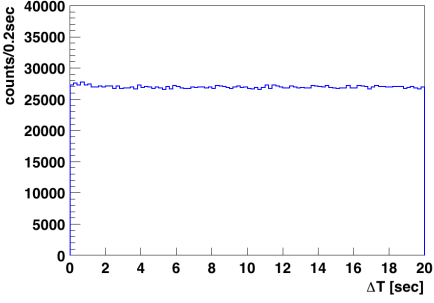
Spallation Products and Muon Cuts

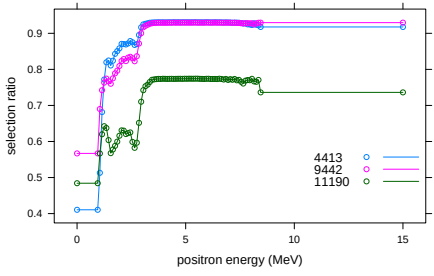
- spallation from cosmic μ, n rich: 2ms cut
- $^{8}\mathrm{He}$, $^{9}\mathrm{Li}$ by showering μ $\beta^{-}\mathrm{n}$ decay, mimic $\bar{\nu}_e$ signal: 2s cut
- left: showering μ, right: 3m around well-reconstructed μ track



Accidental and Heuristic Selection

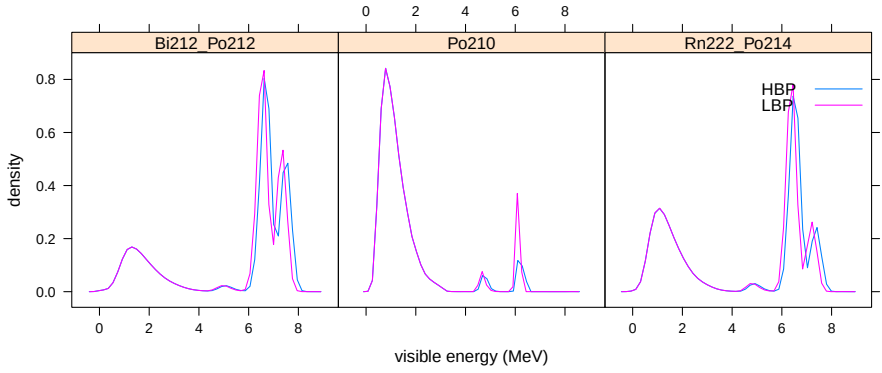
- random coincidence by natural radioactivity
  high activity in low energy, scaled from off-time window
- heuristic selection
  cut on likelihood ratio $\mathcal{L}_\nu/\mathcal{L}_{acc}$





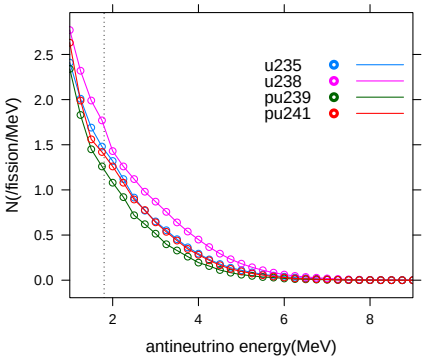
Alpha-Neutron Scattering

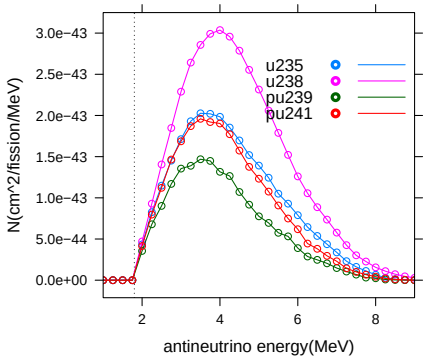
- α from $^{210}\mathrm{Po}$, $^{13}\mathrm{C}(\alpha,\mathrm{n})^{16}\mathrm{O}$
- prompt: α, $^{16}\mathrm{O}^{*}$, n-p elastic scattering, mimic $\bar{\nu}_e$
- $\propto$ rate of α decay, but large uncertainty in cross section.
- $^{210}\mathrm{Po}^{13}\mathrm{C}$ calibration



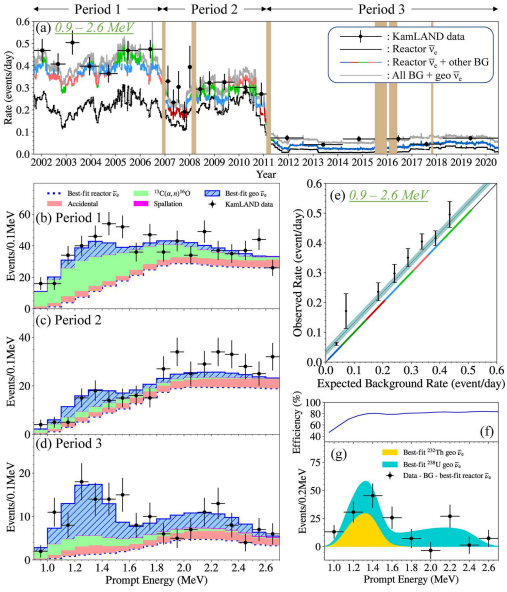
Reactor Neutrino

- constraint by higher energy of E^+ 2.6-8.5MeV
- affected by reactor fission model and neutrino oscillation parameter



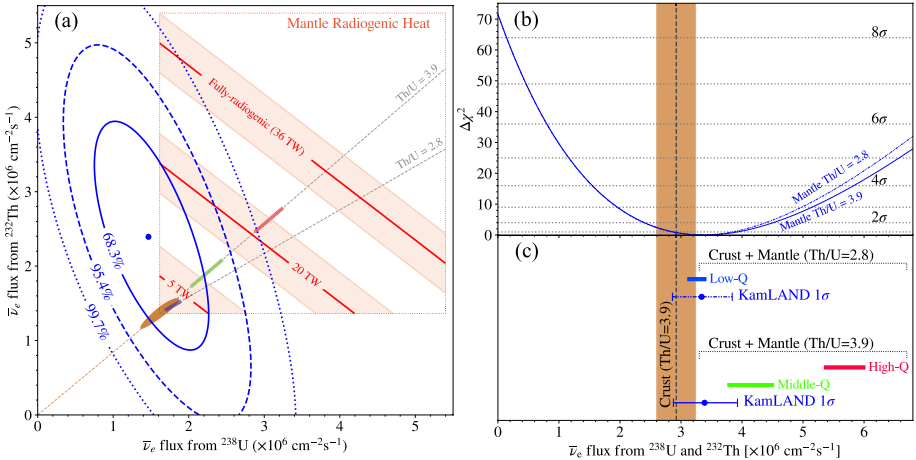


Geoneutrino measurement from KamLAND



- After the shutting down of nuclear reactors in Japan since 2011, geoneutrino S/N ratio at KamLAND boosted.

Flux measurement

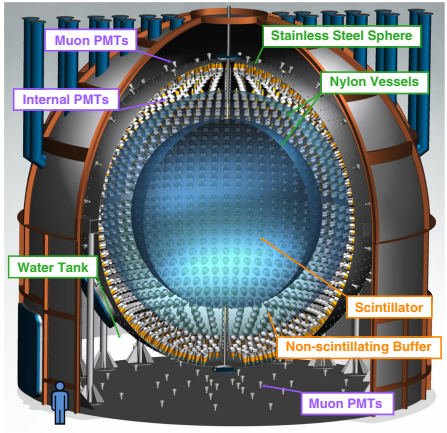


- High-Q model is disfavored.
- Geoneutrino gives strong constraints to Geological models.

Borexino

Borexino: an underground liquid-scintillator detector

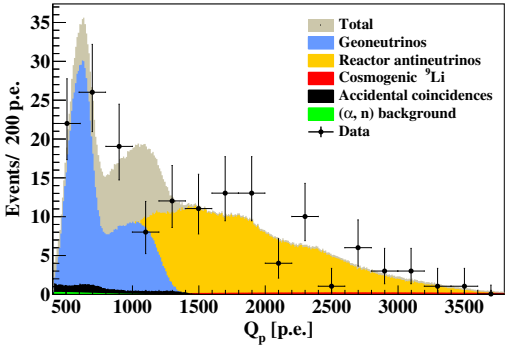
PRD 101, 012009 (2020), Fig. 2



- Gran Sasso, Italy; 3800 m water-equivalent overburden.
- 278 t nominal liquid-scintillator target.
- Low backgrounds: purification, buffer shielding, water-Cherenkov muon veto.
- Energy: $\sigma_E/E \simeq 5\%/\sqrt{E/\mathrm{MeV}}$
- Vertex: $\sim$10 cm at 1 MeV (central).

Separating geoneutrinos from reactor backgrounds

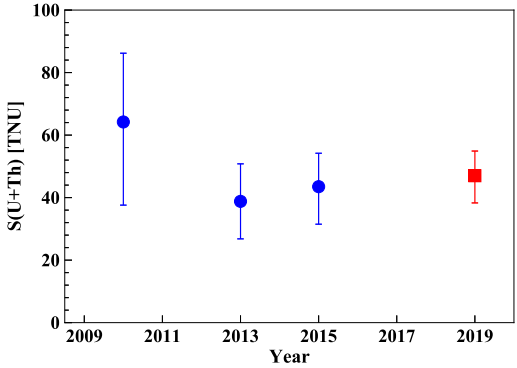
PRD 101, 012009 (2020), Fig. 48(a)



- Dec. 2007–Apr. 2019; 154 IBD candidates.
- Free: geoneutrinos and reactor $\bar{\nu}_e$.
- Constrained: non-$\bar{\nu}_e$ backgrounds.
- Fixed Th/U mass ratio: 3.9.
- Q_p: prompt charge (energy).

The geoneutrino signal at Gran Sasso

PRD 101, 012009 (2020), Fig. 51

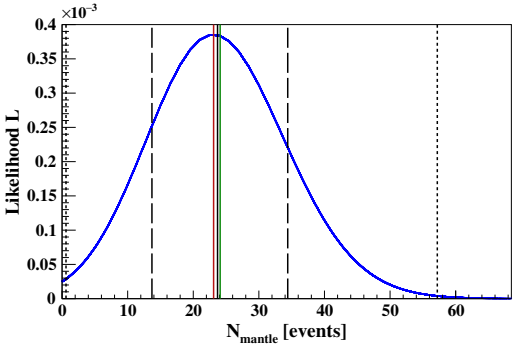


- Red: 2007–2019 data; Th/U mass ratio fixed to 3.9.
- statistical: limited event count.
- systematic: e.g. calibration and efficiency.
- One terrestrial neutrino unit (TNU): one IBD event per 10^{32} free protons per year, at 100% efficiency.

$$S_{\text{geo}} = 47.0^{+8.4}_{-7.7}\,(\text{stat})^{+2.4}_{-1.9}\,(\text{sys})\ \text{TNU}.$$

Agostini et al. (2020), Table XVII.

Inferring the mantle contribution



- Fixed mantle Th/U mass ratio: 3.7.
- No-mantle-signal hypothesis rejected at 99.0% confidence.
- Dashed/dotted: 68%/99.7% intervals.

$$S_{\mathrm{mantle}} = 21.2^{+9.5}_{-9.0}\,(\mathrm{stat})^{+1.1}_{-0.9}\,(\mathrm{sys})\ \mathrm{TNU}.$$

Mantle signal from a spectral fit with a lithosphere constraint.

PRD 101, 012009 (2020), Fig. 52(b), Table XVII.

SNO+

The SNO+ detector

SNOLAB, Sudbury, Canada
SNO's 12 m heavy-water vessel now holds 780 t of scintillator, 2.07 km underground.

1 MeV electrons at the detector centre

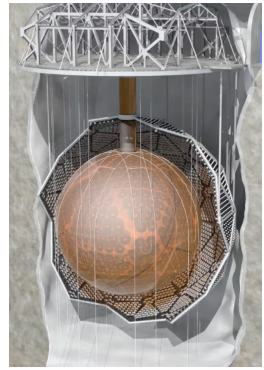
Response	2022–23	2023–25
PMTs hit per MeV	210	320
Energy resolution σ_E/E	6.5%	5.0%

A wavelength shifter was added for the second period.

The 2020 partial fill gave about 300 detected photoelectrons (PE) per MeV of deposited electron energy.

Vertex resolution at the centre was 12 cm per axis for 2.5 MeV electrons in 2022–23.

SNO+ (2021), Fig. 3 (2024) (2025) (2026), Table I.

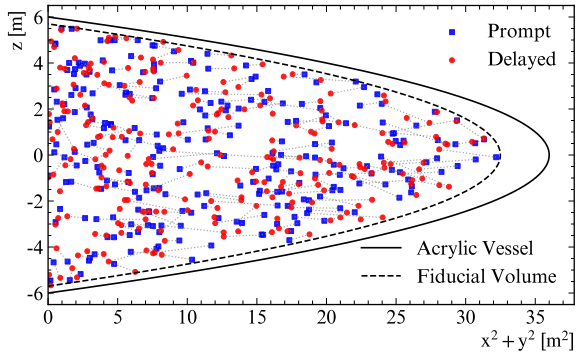


9,362 inward-facing photomultiplier tubes (PMTs). Light concentrators give 54% effective coverage.

Event selection

SNO+ selected **246 pairs** in 2022–25. Both flashes had to lie within 5.7 m of the centre.

Pairing unrelated flashes from the same hour gives fewer than one accidental pair per data set.



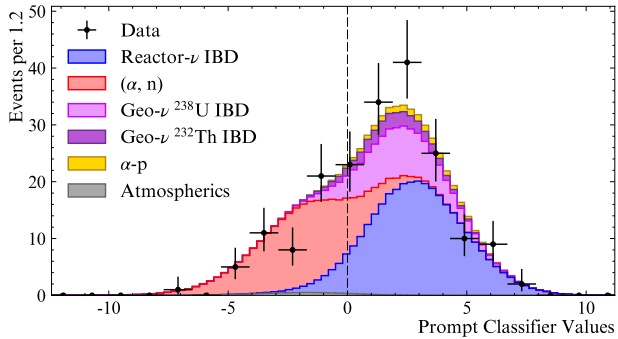
Dotted lines connect the two flashes in each pair.

SNO+ (2026), Fig. 1.

Neutron backgrounds

A neutron from $^{13}\mathrm{C}(\alpha, n)$ can scatter off several protons. Their light arrives with a different time profile from a positron's.

A cut on this timing pattern keeps **90%** of simulated geoneutrinos. In the brighter sample, only **8%** of (α, n) events below 3.5 MeV pass.



The fit uses events to the right of the dashed line.

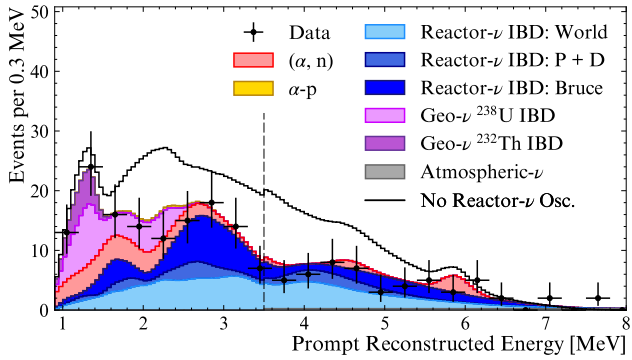
SNO+ (2026), Fig. 4.

The geoneutrino spectrum

Of the 185 selected pairs, the fit attributes about **35** to U and Th.

Exposure (kt yr)	**U+Th rate** (TNU)
0.29	73^{+47}_{-43}
1.46	48^{+14}_{-12}

The full sample includes the earlier data and gives 3.6σ evidence for geoneutrinos.



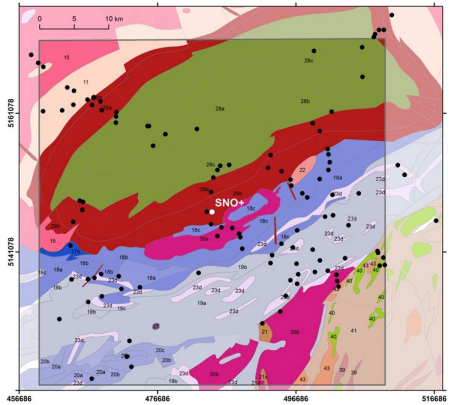
U and Th (purple) end near 2.5 MeV in prompt energy. The reactor spectrum (blue) extends higher.

SNO+ (2025); SNO+ (2026), Fig. 2.

The crust around Sudbury

The mapped part of the upper crust contributes $7.7^{+7.7}_{-3.0}$ TNU. The prediction for the whole crust is $31.1^{+8.0}_{-4.5}$ TNU.

U and Th concentrations vary widely in the nearby Huronian rocks. This limits how well the mantle contribution can be inferred.



Rock samples around SNO+. The inner square spans 50×50 km.

Strati et al. (2017), Fig. 2.

Geoneutrino Detection

KamLAND

Borexino

SNO+

Upcoming

JUNO

JNE

OBD

$\bar{\nu}$ Directionality

Towards ^{40}K

e^- elastic

Gas TPC

ν-nuclei capture

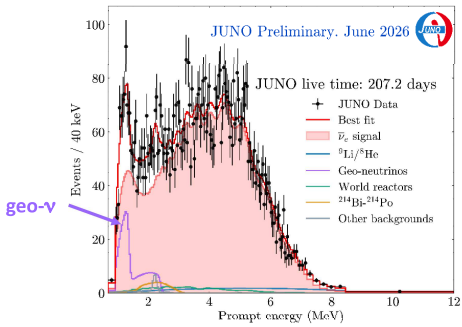
Low-threshold IBD

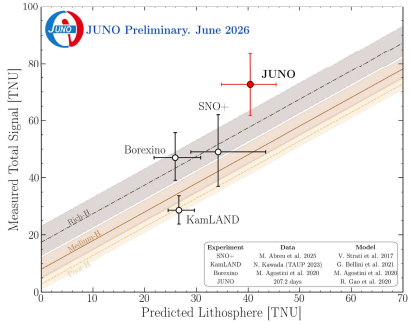
Summary

Upcoming

JUNO will carry geoneutrino measurement to the next level

- Fits are performed without constraint on geo-neutrino flux, but with 3.4±10% U/Th ratio
- JUNO result is higher than expectation from existing models, but not statistically significant

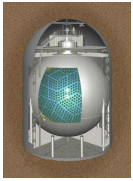




To be covered by Jiajie tomorrow.

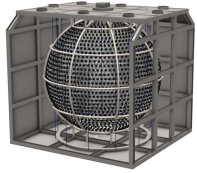
Future geoneutrino sites

KamLAND2
Japan



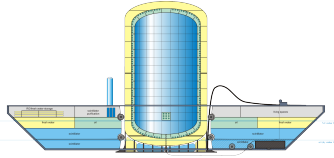
A longer run would reduce the statistical uncertainty at Kamioka.

Jinping
China



Jinping sits above thicker crust than Kamioka. Its distant reactors give a smaller background.

Ocean Bottom Detector
Pacific Ocean



The proposed 1.5 kt detector could move between Pacific sites at about 4 km depth.

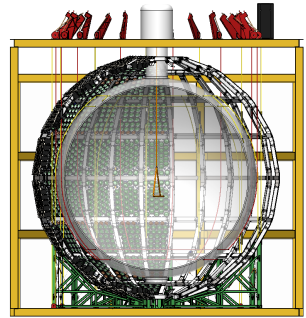
McDonough (TAUP 2025), slide 9. OBD design goal, Hosoya (Neutrino 2026).

The Jinping detector

Jinping, Sichuan, China
The 500 t detector passed design review in 2024. The CJPL-II site lies beneath 2.4 km of rock.

Scintillator forecast
500 PE/MeV and 4.4% energy resolution at 1 MeV visible energy.

Water commissioning simulation
At 5 MeV and 18% photocathode coverage, the energy resolution is 27.4% and the vertex resolution is 60 cm along one axis.



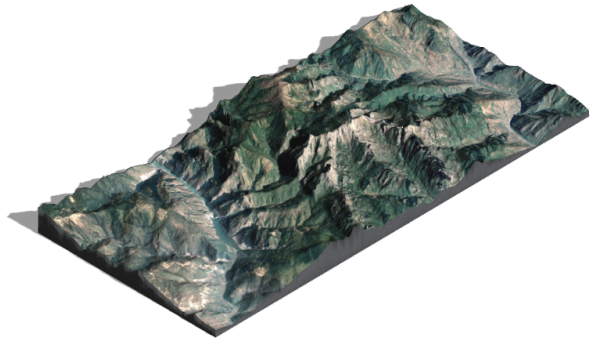
9.96 m acrylic sphere. About 3,000 eight-inch PMTs give about 40% coverage with concentrators.

JNE (TAUP 2025), slides 10 and 22; Meng & Zhang (2026).

The Jinping site

The mountain shields the lab from cosmic-ray muons. The nearest power reactors are about **1,000 km** away.

With 500 t of scintillator, JNE expects tens of geoneutrino events in 5 years.

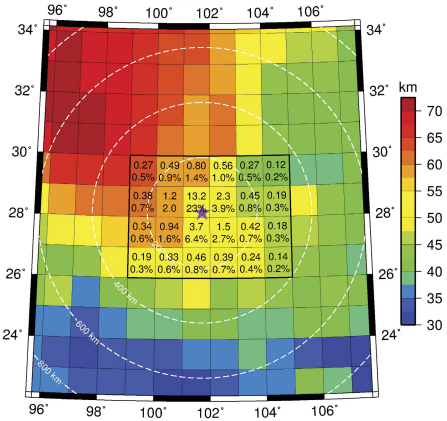


JNE (TAUP 2025), slides 4 and 6.

The crust around Jinping

Jinping lies at the star. The crust thickens to the northwest, toward the Tibetan Plateau.

About half of the expected signal comes from within 300 km. Its size depends on the thickness of the local rock layers and their U and Th content.



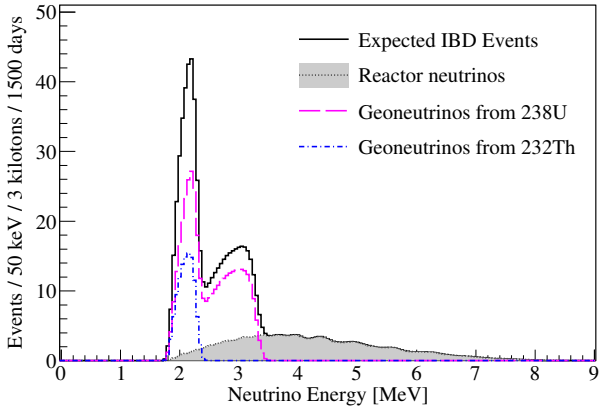
Colour gives crustal thickness. Each tile lists its predicted contribution.

Šrámek et al. (2016), Figs. 1 and 3.

The expected spectrum

Wan et al. assume $3\ \mathrm{kt} \times 1{,}500$ live days. They predict **527 U+Th events** and about 60 reactor events between 1.8 and 3.3 MeV.

Above 3.3 MeV, the reactor tail constrains the background. The forecast precision is 4.6% on U+Th and 26.3% on the Th/U event ratio.



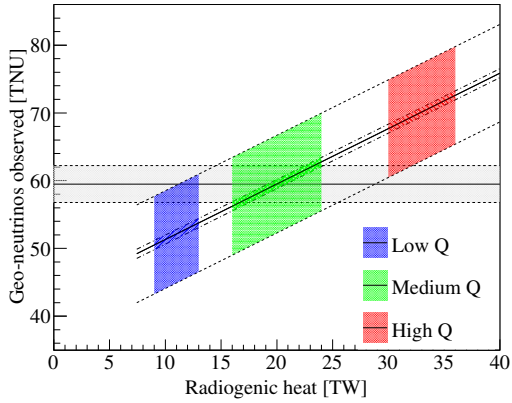
The same mass exposure takes 9,000 live days with a 500 t fiducial target.

Wan et al. (2017), Fig. 5 and Tables VI–VII.

Radiogenic heat

Source	U+Th (TNU)
Crust	49.0 ± 7.3
Mantle	10.4 ± 2.7

The crust uncertainty is comparable to the mantle signal. Inferring mantle heat from the remaining rate requires assumptions about Th/U and K/Th.



The grey band is the projected rate. The colours show Earth models with different heat production.

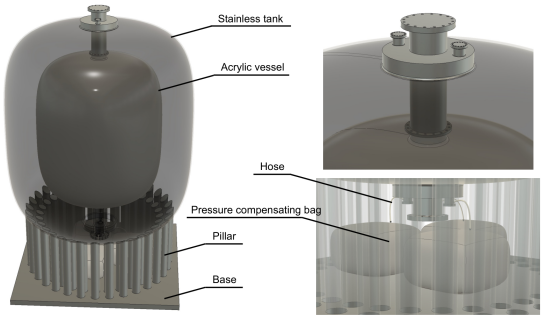
Wan et al. (2017), Fig. 6 and Table V.

The Ocean Bottom Detector

Tohoku University and JAMSTEC began developing OBD in 2019. The proposed site is on the Pacific seafloor off Hawaii.

1.5 kt liquid-scintillator design

Water depth	about 4 km
Steel tank	18 m wide, 20 m tall
Light sensors	about 3,000 PMTs
Light-yield target	450 PE/MeV

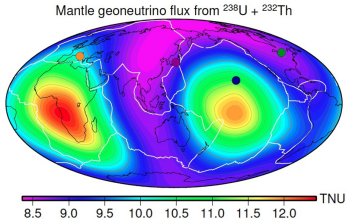


The acrylic vessel holds the scintillator. A 3 m oil buffer shields it from radioactivity in the sensors and tank.

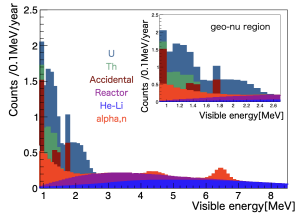
Sakai et al., OBD design. Araki et al. (2026), Fig. 7.

Measuring the mantle signal

Where to measure



1.5 kt off Hawaii



Oceanic crust contains less U and Th. The predicted mantle share rises from 21% at Kamioka to 81% at $9°$S, $161°$W.

The simulation gives 8.2 geoneutrinos per year, including 5.8 from the mantle. Reactors, accidental pairs and (α, n) add 6.4 events in the window.

Fit the U+Th energy spectrum and subtract the expected crust rate. For an intermediate-heat mantle, three years give a projected 3.5σ sensitivity to a nonzero mantle signal.

Šrámek et al., Table 6. McDonough, TAUP 2025. Sakai et al., Fig. 2. Watanabe (2025), rates.

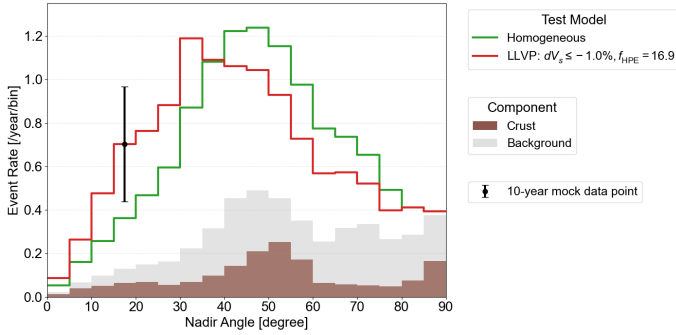
Where mantle geoneutrinos come from

South Pacific simulation

At one 1.5 kt site, the two models give almost the same total, including backgrounds.

Uniform mantle
15.4 events/yr

U/Th-rich region deep below the site
15.3 events/yr



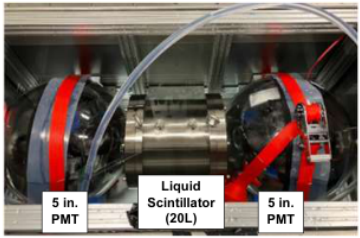
0° is straight down. The enriched region adds events at small nadir angles. The black point illustrates a simulated ten-year sample.

With 20° angular resolution and 20 years of data, this enrichment model could be distinguished from a uniform mantle at 2.6σ.

Xu et al. (2026 preprint), Figs. 3, 5 and Table 3. OBD Consortium, PoS(TAUP2025)315. Xu, Neutrino 2026.

Testing the OBD prototype

20 L prototype



Two 5-inch PMTs read the scintillator. A land test of the assembled prototype recorded light from a ^{60}Co source.

Pressure compensation



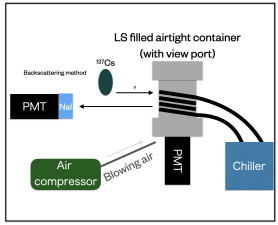
A liquid-filled hose flexes as pressure rises. The vessel and hose passed a pressure-tank test equivalent to 1 km of water.

At Neutrino 2026, the team presented its plans to monitor light output at 1 km depth off Hatsushima, Japan.

Watanabe et al. (2023), OBD design. T. Araki, prototype tests (thesis). Hosoya, Neutrino 2026 (photos).

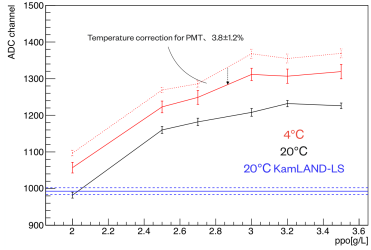
Scintillator light yield at $4\,^{\circ}\mathrm{C}$

100 mL laboratory sample



A sodium iodide crystal tags backscattered ^{137}Cs photons. This selects recoil electrons of nearly the same energy at both temperatures.

Measured light output

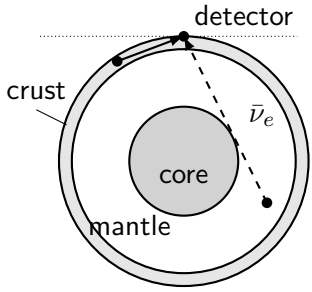


At 3 g/L of the fluor PPO, the sample gave **8.6% more light** at $4\,^{\circ}\mathrm{C}$ than at $20\,^{\circ}\mathrm{C}$ after correcting for the PMT response.

Sakai et al., J. Phys.: Conf. Ser. 2156, Fig. 5. Araki et al. (2026), Fig. 4.

$\bar{\nu}$ Directionality

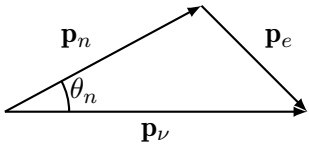
Why neutrino direction matters



- Energy spectra alone: limited spatial information
- Crust–mantle separation; mantle radiogenic heat
- Tests of mantle U/Th heterogeneity
- Solar-background rejection in electron scattering

Physics motivation: Leyton et al. (2017); Tanaka and Watanabe (2014).

Why IBD neutrons go forward



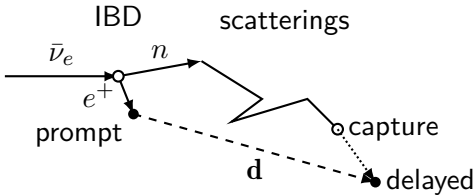
- Free proton initially at rest; $c = 1$.
- E_ν: incident antineutrino energy.
- m_e: positron mass.
- $\Delta = m_n - m_p$: neutron–proton mass difference.

$$\mathbf{p}_\nu = \mathbf{p}_e + \mathbf{p}_n,$$
$$|\mathbf{p}_e| \leq \sqrt{(E_\nu - \Delta)^2 - m_e^2} < E_\nu.$$

The neutron must carry forward momentum, even when the positron does not.

Vogel and Beacom, PRD 60, 053003 (1999), Sec. IV, Eqs. (26)–(27).

Anti-neutrino directionality



- Prompt: reconstructed e^+ position.
- Delayed: reconstructed n-capture position.
- Scattering and reconstruction blur individual events.
- Mean displacement follows neutrino flight; the source lies opposite.

$$\mathbf{d} = \mathbf{r}_{\text{delayed}} - \mathbf{r}_{\text{prompt}}.$$

Vogel and Beacom, PRD 60, 053003 (1999), Sec. IV; PROSPECT (2025), Secs. II and IV.

MCMC source-direction inference

Use Markov Chain Monte Carlo hammer to hit hard inference problems.

Per candidate i:

$$\Delta t_i = t_{d,i} - t_{p,i}, \quad \Delta r_i = \|\mathbf{d}_i\|.$$

For a trial direction $\hat{\boldsymbol{\mu}}$:

$$c_i = \hat{\mathbf{d}}_i \cdot \hat{\boldsymbol{\mu}} = \cos\theta_i.$$

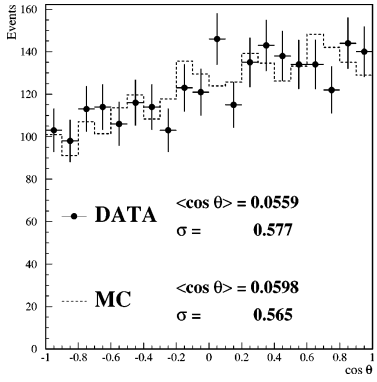
$$\mathcal{L}(\hat{\boldsymbol{\mu}}) = \prod_i R(c_i(\hat{\boldsymbol{\mu}}) \mid \Delta r_i, \Delta t_i)\,,$$

- Simulation gives the response $R(c \mid \Delta r, \Delta t)$.
- MCMC samples the direction posterior.
- $\Delta r, \Delta t$ keep information a plain vector average discards.

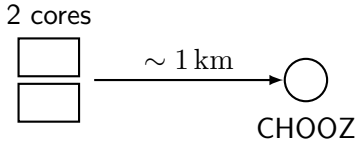
$$p(\hat{\boldsymbol{\mu}} \mid \text{data}) \propto p(\hat{\boldsymbol{\mu}})\,\mathcal{L}(\hat{\boldsymbol{\mu}}).$$

CHOOZ: statistical reactor pointing

PRD 61, 012001 (2000), Fig. 4, Table II



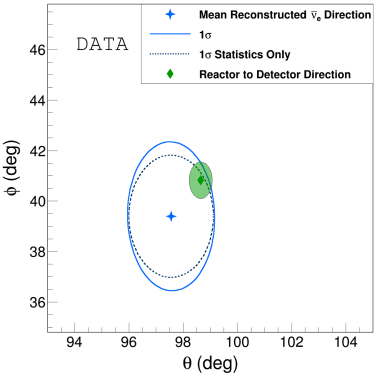
θ: displacement vs neutrino-flight angle. Points: data; dashed: simulation.

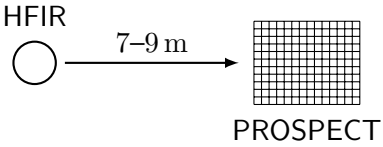


- $\sim$2500 selected reactor-on candidates.
- Mean forward displacement: 1.9 ± 0.4 cm.
- Source direction: 18° half-cone, 68% confidence.
- Statistical pointing, not single-event angular resolution.

PROSPECT-I: localized neutron capture

PRD 111, 032014 (2025), Fig. 7





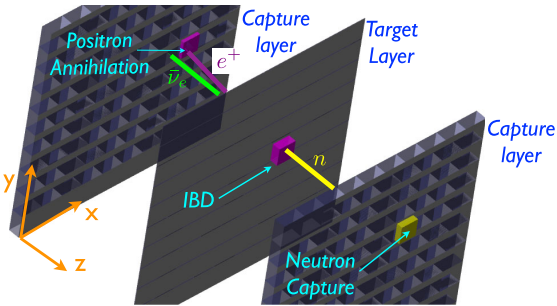
- Segmented ^{6}Li target; localized neutron capture.
- About 48,000 IBD signals after background subtraction.
- Azimuth $\phi = (39.4 \pm 2.9)^\circ$.
- Zenith $\theta = (97.6 \pm 1.6)^\circ$.

Ellipses: 1σ; dotted: statistics only.

$$^6\mathrm{Li} + \mathrm{n} \longrightarrow \alpha + {}^3\mathrm{H}$$

Preserving the neutron direction

SANTA: segmented antineutrino tomography apparatus.
PRL 114, 071802 (2015), Fig. 1



- Thin target: minimize neutron scattering before escape.
- Low-density gap separates target and capture layers.
- Boron-loaded scintillator captures the neutron.
- Design and simulation study.

Reactor pointing is demonstrated; geoneutrino imaging still requires large exposures and background control.

$$^{10}\mathrm{B} + \mathrm{n} \longrightarrow {}^{7}\mathrm{Li} + \alpha + \gamma\,(0.48\,\mathrm{MeV})$$

Detector designs and geoneutrino prospects

Approach	Directional handle	Status
^{6}Li, segmentation	Local neutron capture	PROSPECT: data; SANDD: prototype/simulation Sutanto et al. (2021)
Thin target + gap (SANTA)	Less neutron scattering	Design/simulation

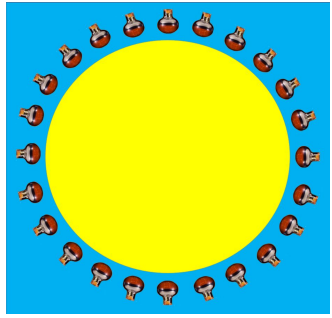
- Compare geometry, position response and usable directional samples (Duvall et al. 2024).
- Geoneutrino prospects with model-dependent crust/mantle patterns (Tanaka and Watanabe 2014) and ocean-bottom mantle studies (Xu et al. arXiv:2606.13273).

Towards ^{40}K

A slow scintillator detector

Potassium study at Jinping
The simulation assumes 50% photocathode coverage, about 30% quantum efficiency for visible light and a 7 ns scintillation rise time.

QiScinT detector simulation
A separate 500 t oil-based detector has a 7.7 ns rise time and 376 detected PE/MeV. At 2 MeV the simulated electron energy resolution is 4.1% and the vertex resolution is 9.2 cm along one axis.



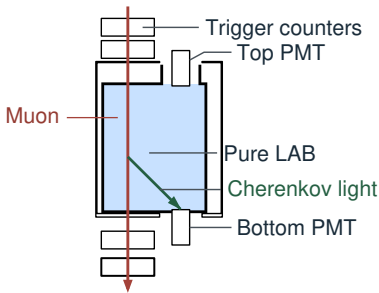
Slow scintillator (yellow) inside the water shield (blue) in the 2017 proposal.

Wang & Chen (2020), Fig. 4; Luo et al. (2023); Sun et al. (2026), Sec. 3.

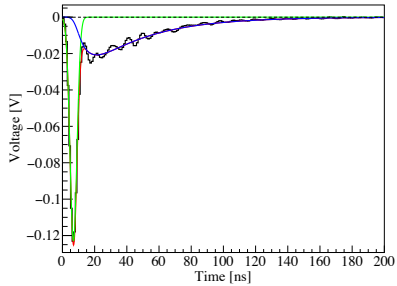
Slow scintillator timing

Four counters tag muons crossing the liquid. Both PMTs collect scintillation light.

Muon telescope



Bottom PMT waveform



- In pure linear alkylbenzene (LAB), the bottom PMT also sees a prompt Cherenkov pulse (green). The scintillation tail (blue) decays in $36.6±2.4$~ns.
- Aqueous LiCl + 1 ppm carbostyril 124 gave 3.7 ± 0.4 (top) and 16.0 ± 1.6 (bottom) PE/muon.

Li et al. (2016), Figs. 2 (adapted), 9. Liang et al. (2023), Table 1.

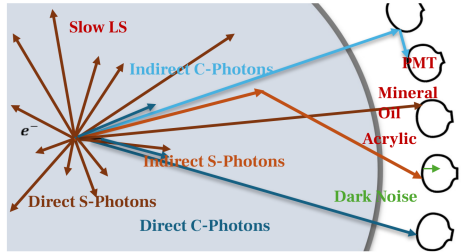
Electron direction with QiScinT

QiScinT fits each electron's kinetic energy, vertex, time and direction, $\Theta = (E, \mathbf{r}, t_0, \hat{\mathbf{u}})$.

PMT i detects n_i photoelectrons at times t_{ij}.

$$\mathcal{L}(\Theta) = \prod_i \Bigg[\underbrace{\pi(n_i \mid \lambda_i)}_{\text{PE count}} \prod_{j=1}^{n_i} \underbrace{f_i(t_{ij} \mid \Theta)}_{\text{arrival time}} \Bigg].$$

$\lambda_i(\Theta)$ is the expected PE count. f_i is the arrival-time density. Early Cherenkov light favours PMTs on the cone around $\hat{\mathbf{u}}$.



Direct and indirect light paths. Blue arrows show Cherenkov light.

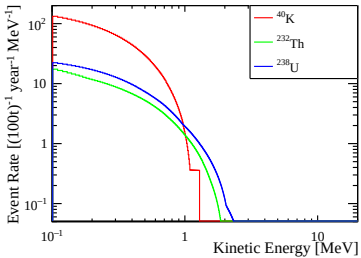
Potassium simulation

Averaging photon directions from the first 2~ns of emission gave 40° angular resolution at 1~MeV (68\

Luo et al. (2023), Eq. 5.1. JNE (TAUP 2025), slide 19. Sun et al. (2026), Fig. 11.

Selecting potassium recoils

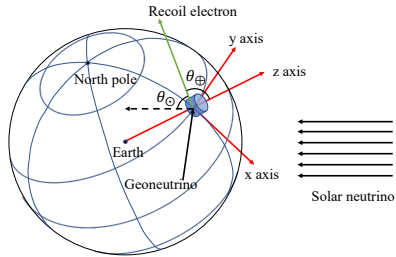
Electron energy



The main ^{40}K branch produces electron recoils up to 1.1 MeV. The 0.7 MeV cut removes most solar ^{7}Be recoils.

Sun et al. (2026), Figs. 5 and 1, Table 1.

Direction relative to the Sun

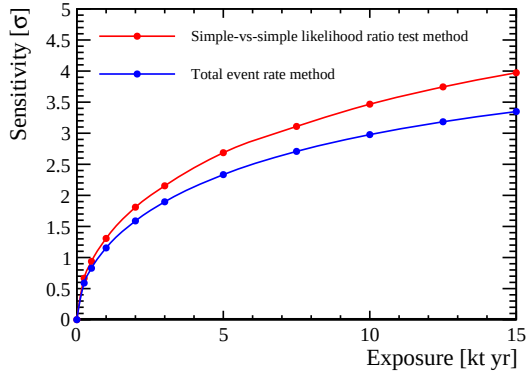


Remove recoils pointing along the incoming sunlight. The cut keeps **43% of K** and **2% of solar** events in the window.

Geoneutrino sensitivity

At 5 kt yr, about 40 potassium and 40 U+Th events survive, alongside 748 solar and 112 radioactive events.

The directional fit reaches 3σ for **K+U+Th** at **6.9 kt yr**. A test for potassium alone would allow U and Th in both fits.

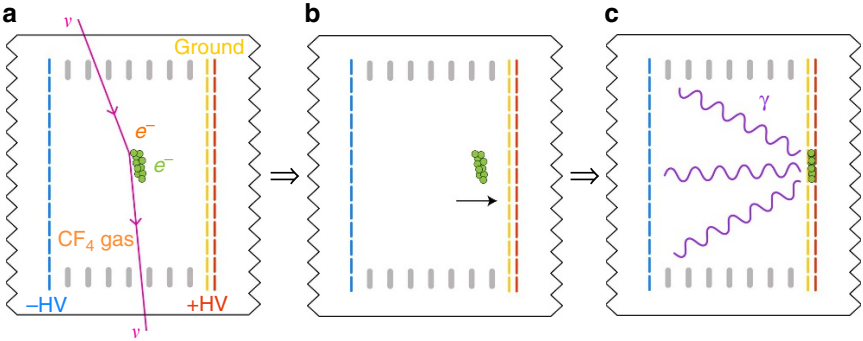


The red curve uses recoil directions. The blue curve uses the event count.

Sun et al. (2026), Fig. 18(b) and Table 1.

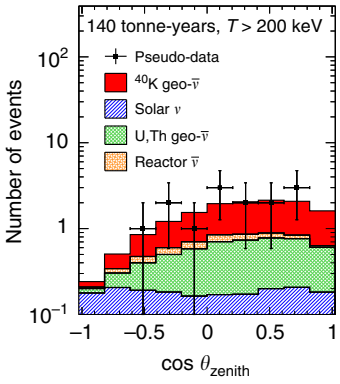
Gas TPC

Leyton et al., Nat. Commun. 8, 15989 (2017), Fig. 3



- ^{40}K antineutrino endpoint $\simeq 1.3\,\mathrm{MeV}$, below the $1.8\,\mathrm{MeV}$ IBD threshold.
- $\bar{\nu}_e + e^- \to \bar{\nu}_e + e^-$: recoil energy and direction.
- $\mathrm{CF_4}$ gas time projection chamber (TPC) with ionization track, drift, then amplification/readout.

Gas TPC: projected K-40 signal

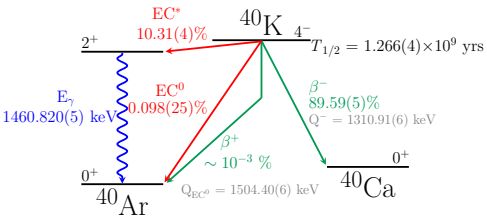


- CF_4 at Gran Sasso: 140 tonne-years; recoil kinetic energy $T > 200\,\text{keV}$.
- Solar-direction rejection applied; other neutrino backgrounds remain.
- Assumed electron angular resolution: $\sigma_\theta = 102°(T/\text{keV})^{-0.361}$, extrapolated from MUNU at 1 bar CF_4.
- Assumes 100% track efficiency above threshold and negligible non-neutrino backgrounds.

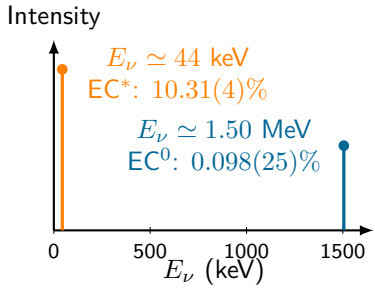
Leyton, Dye and Monroe (2017), Fig. 5(a), Eq. (1), Methods and Discussion.

^{40}K EC

Decay scheme



ν_e spectrum (schematic)



3-folds signature of ^{40}K, all of which are hard to detect!

[1] L. Hariasz *et al.*, *Phys. Rev. C* **108**, 014327 (2023).

Solar ν charged-current observatory

- A solar neutrino charged-current interaction might be able to see the monochronic line of ^{40}K EC.
- Unfortunately, 44 keV is under most of CC isotope candidates.
- The 1.5 MeV branching ratio is less than $0.1\,\%$.

Co-development of extreme solar and geoneutrino detection technology

Doped liquid-scintillator that can do ν_e spectrometry.

- ^{100}Mo, ^{150}Nd are on the table.

Liquid 3 He

$$^3\mathrm{He} + \bar{\nu}_e \longrightarrow {}^3\mathrm{H} + \mathrm{e}^+$$

- Q=0.0186 + 0.511x2, just below ^{40}K β decay endpoint.
- The charged-current capture of $\bar{\nu}_e$ need to pay for the e^+ tax. Very challenging to find a detection isotope.

Summary

Summary

1. The golden era of geoneutrino has come. Multiple new experiments came online forming a global geoneutrino network.
2. Extract more insights on geological models from geoneutrinos
   - Fiducial volume;
   - Cosmogenic background;
   - Reactor neutrino (better constrain, move a away, shutdown, etc.)
   - Local crustal modeling (geological community)
3. Next major milestones of new technology of geoneutrino detection
   - directionality;
   - to the ocean bottom;
   - ^{40}K co-development with next-generation solar ν programs.

Thanks for your attention!

Backup

Reactor detection in liquid scintillator

Ideal detector

The model considers a reactor with 50 MW of thermal power. The backgrounds are other reactors and geoneutrinos.

The analysis keeps antineutrinos with $E_\nu > 3.3$ MeV. Geoneutrinos from U and Th fall below this cut.

Fiducial mass and live time

Distance	Low background	High background
10 km	1 kt, 1 month	1 kt, 4 months
20 km	1 kt, 5 months	5 kt, 1 year
50 km	10 kt, 1 year	1,000 kt, 1 year
100 km	100 kt, 1 year	Out of reach

Out of reach within one year in this model.

Reactor detection in gadolinium-loaded water

Simulated detector

For the same 50 MW reactor, the simulation tracks light to photomultiplier tubes covering 40% of the detector surface and reconstructs each event.

Backgrounds include other reactors, geoneutrinos, ambient radioactivity, and muon-induced neutrons, pions and gamma rays.

Fiducial mass and live time

Distance	Low background	High background
10 km	Not studied	1.4 kt, 1 year
20 km	1.4 kt, 1 year	25 kt, 1 year
35 km	60 kt, 1 year	Out of reach
100 km	Out of reach	Out of reach

Out of reach within one year with this design.

To measure U and Th, we keep the low-energy events and fit the reactor contribution.